Thin Microwave Absorber Based on Laser-Induced Graphene Frequency Selective Surfaces

Yann Houeix, *Student Member, IEEE*, Francisco J. Romero, Francisco G. Ruiz, Diego P. Morales, Noel Rodriguez, and Darine Kaddour, *Member, IEEE*

***Abstract*—This study presents a pioneering approach to fabricating single-layer Frequency Selective Surfaces (FSS) using Laser-Induced Graphene (LIG). The FSS structure proposed consists of periodic resistive patterns of LIG synthesized through a one-step laser photothermal process directly on the surface of a thin polyimide substrate. The structural and electrical properties of LIG were thoroughly investigated to develop an electrical model aiming at optimizing the design and absorbing properties. After that, a 12 mm thick LIG-FSS microwave absorber prototype was fabricated and tested under real conditions, demonstrating over 90% absorption in the frequency band from 1.69 to 2.91 GHz with a thickness of only 0.068 times the maximum wavelength (λ_{max}), demonstrating good agreement with the simulations and theoretical results. Additionally, we discuss the tunability of the frequency response of the absorber by adjusting accordingly the induced material's properties. Finally, we also demonstrate the versatility of this approach for the fabrication of FSS structures based on alternative patterns. The findings presented in this work highlight the promising potential of sustainable microwave absorbers based on LIG-FSS structures.**

***Index Terms*—Frequency selective surfaces, laser-induced graphene, microwave absorber, thin-film electronics.**

I. Introduction

MICROWAVE absorbers have gained significant attention in various applications fields, including military uses and everyday applications, such as stealth technology and anechoic chambers [1]. In addition, with the rise of the Internet of Things (IoT) and the increasing number of wireless devices exchanging data remotely, electromagnetic (EM) radiation pollution has become a significant concern. Consequently, there is a rising interest in advanced materials and structures designed to absorb microwave energy effectively [2]. Among them, resistive patterned Frequency Selective Surface (FSS) absorbers are attracting increasing attention due to their superior performance compared to traditional radar absorbers like Salisbury and Jaumann screens. FSS structures offer enhanced absorption efficiency with reduced volume, overcoming the thickness-bandwidth ratio limitation of other alternatives [1]. The precise design of the FSS geometric characteristics enables the adjustment of the surface impedance to achieve different filtering characteristics, such as low-pass, band-pass, or band-stop filters [3]. One of the desired features for FSS structures is the capability to tune their frequency of resonance and/or their bandwidth, typically achieved by altering material properties or incorporating concentrated/distributed elements [4], [5], [6]. This latter alternative is the most common in traditional implementations based on printed circuit boards (PCB). However, introducing additional elements to tune the FSS may result in increased size, weight, and complexity. Therefore, the most promising advances in FSS technology have been made possible thanks to the introduction of new materials, such as conductive inks and carbon-derived metamaterials, as well as innovative fabrication techniques like screen-printing or inkjet printing [7], [8], [9]. These advancements have led to the production of diverse FSS structures, including multilayers and multiple resistive patterns with unique features, including transparency, tunability, lightweight, and flexibility [10], [11], [12]. Therefore, these structures have potential applications beyond the scope of microwave and optical frequency filters and radar absorber materials, extending to chipless Radio-Frequency Identification (RFID) wearable sensors and other applications with irregular surfaces [13], [14], [15]. The potential of FSS in RFID applications has already been demonstrated as a successful approach for improving the electrical performance of RFID antennas, including enhancements in reading range, interference mitigation and reduction of power losses [16], [17]. For instance, Lazaro et al. proposed the use of active FSS to reduce both Radar Cross-Section (RCS) area and backscattering in ultrawideband (UWB) semi-passive RFID tags [18]. Similarly, Jiménez-Sáez et al. introduced a FSS model to reduce the RCS and enhance the reading range of chipless RFID tags with reduced power consumption [19]. The use of FSS to improve the reading range of RFID tags with enhanced gain and electromagnetic interference immunity

Manuscript received 30 December 2023; revised 29 January 2024; accepted 9 February 2024. Date of publication 20 February 2024; date of current version 7 May 2024. This work was supported in part by MCIN/AEI/10.13039/501100011033 under Grant PID2020-117344RB-I00 and Project TED2021-129949A-I00; in part by the FEDER/Junta de Andalucía-Consejería de Transformación Económica, Industria, Conocimiento y Universidades under Project P20_00265 and Project BRNM-680-UGR20; in part by the European Union NextGenerationEU/PRTR; in part by the Junta de Andalucía – Consejería de Transformación Económica, Industria, Conocimiento y Universidades under Project ProyExcel-00268; and in part by the Spanish Ministry of Sciences and Innovation through the Predoctoral Grant under Grant PRE2021-096886. Funding for open access charge: Universidad de Granada/CBUA. *(Corresponding author: Yann Houeix.)*

Yann Houeix, Francisco J. Romero, Francisco G. Ruiz, Diego P. Morales, and Noel Rodriguez are with the Department of Electronics and Computer Technology, University of Granada, 18071 Granada, Spain (e-mail: yannhx@ugr.es; franromero@ugr.es; franruiz@ugr.es; diegopm@ugr.es; noel@ugr.es).

Darine Kaddour is with the Laboratoire de Conception et d'Intégration des Systèmes, Grenoble INP, University of Grenoble Alpes, 26902 Valence, France (e-mail: darine.kaddour@lcis.grenoble-inp.fr).

Digital Object Identifier 10.1109/JRFID.2024.3368005

was also demonstrated by Sharma et al. [17], [20]. Finally, El-Mahgoub et al. demonstrated that FSS can also be tuned to achieve either total reflection or complete transmission for the entire UHF RFID global band [21].

In recent years, one of the fabrication techniques that is gaining significant interest is based on the laser photothermal treatment of carbon-rich materials to isolate and rearrange their carbon bonds, thus obtaining an amorphous form of nanographene (laser-induced graphene, LIG) with relatively good mechanical, thermal and electrical properties [22]. LIG has been proposed as a sustainable alternative for the fabrication of electronic devices across a wide range of applications, including sensors, energy-storage devices, or antennas, among others [23], [24], [25]. The interest in LIG technology lies in the possibility of achieving complex resistive patterns on the surface of diverse substrates following a single fabrication step at room temperature without requiring lithographic masks or hazardous materials. Furthermore, it also offers the possibility of controlling the conductivity of the resulting material by adjusting the laser parameters accordingly. LIG has been used in many RF applications, such as RFID antennas [26], [27], [28]. All these features make LIG a really promising simple and low-cost contender when it comes to FSS fabrication as we demonstrated in our preliminary experiments [28].

Therefore, as an extension of our preliminary work, this paper presents the optimization of the laser-photothermal process to improve the absorption properties of the FSS structure with an analysis of its working principle and equivalent circuit. Additionally, the versatility of the fabrication process, not only to tune the absorption properties of a specific FSS structure, but also to fabricate FSS structures with multiple diverse patterns and frequency responses is demonstrated.

In particular, after this introduction, Section II presents the design and fabrication procedure of the FSS structure together with the characterization of both structural and electrical properties of the resistive material (LIG). In Section III, these properties are used in a 3D EM simulation software to tune the FSS structure for the desired frequency bands, as well as to obtain the equivalent circuit model of the absorption mechanism. The experimental results of the optimized FSS structure are included in Section IV, demonstrating good agreement with both the electrical model and the EM simulation results. This section also demonstrates the tunability of the frequency response by adjusting the sheet resistance of LIG as well as the potential of the laser photothermal process to produce advanced FSS patterns without increasing the complexity of the fabrication process. Finally, the main conclusions are drawn in Section V.

II. Fabrication and Material Properties

A. FSS Structure Fabrication Process

The proposed absorbing structure is composed of a lossy frequency selective surface over a thin grounded dielectric slab, as illustrated in Fig. 1. The surface consists of a resistive pattern made of LIG directly on top of a *Kapton*® HN polyimide film with a thickness of 150 μm. The dielectric

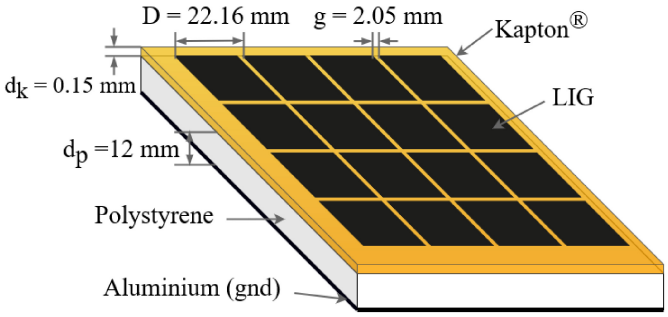

Fig. 1. Structure of the proposed patch LIG-FSS.

spacer is made of 12 mm polystyrene foam, as determined through the optimization process detailed in Section III, while an aluminum plate at the bottom serves as the ground plane.

Among the various typical shapes, such as rings, meanders cells or Jerusalem crosses, square patch elements were selected as they offer better performance for wideband absorbers at fixed frequencies [8]. The patterning of the polyimide surface was carried out using a *Rayjet*® 50 CO_2 laser with an infrared wavelength of 10.6 μm. The laser treatment induces a photothermal effect on the lattice of the substrate, leading to a significant increase of the temperature. As a result, a considerable portion of the weaker bonds (imide and carbonyl) within the polyimide chain are broken [29], hence isolating the carbon bonds while releasing oxygen and nitrogen in the form of gases [25]. This process transforms the insulating substrate into an electrically conductive material by rearranging the polymeric chain into a graphene-derived structure known as LIG. In this case, the polyimide does not introduce any significant effect to the electromagnetic response of the absorber, as its thickness is negligible compared to the thickness of the polystyrene. However, alternative precursors with different properties (thickness and permittivity) could also be explored to add more degrees of freedom to the optimization.

B. Material Characterization

The microstructure of the resulting material, in comparison with the raw polyimide, is presented in the Scanning Electron Microscopy (SEM) image of Fig. 2. As seen, LIG appears on top of the flat surface as a porous foam as a consequence of the laser photothermal process.

The Raman spectrum of the induced material (Fig. 3) confirms its derived-graphene nature through the presence of the characteristic D, G, and 2D peaks located at 1350 cm^{-1}, 1680 cm^{-1}, and 2700 cm^{-1}, respectively. These peaks are commonly observed in graphene and related materials and provide information about their crystallographic quality. The G peak arises from sp^2 hybridized carbon structure, while the D peak is associated with defects and disorders in the lattice structure. Lastly, the 2D peak confirms the graphene-derived nature of the compound. According to the particular characteristics of these peaks, i.e., a ratio $I_G/I_D \approx 1$ and

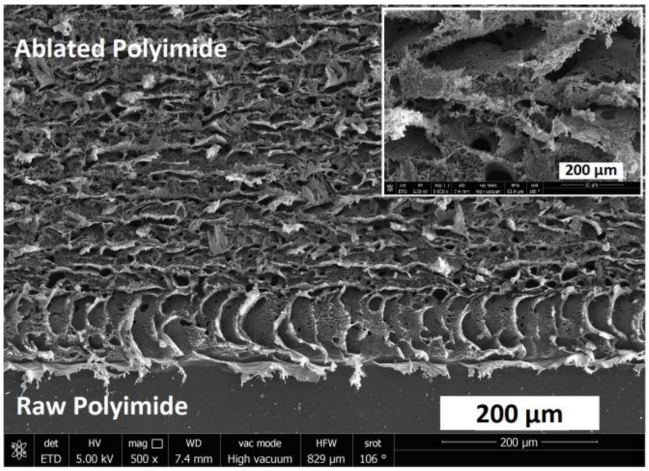

Fig. 2. SEM image of the LIG on the polyimide substrate obtained with a laser power of 12 W at an engraving speed of 200 mm/s.

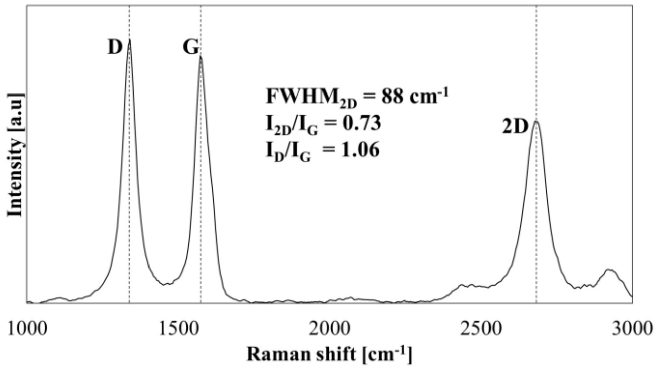

Fig. 3. Raman spectra of the LIG on the polyimide substrate obtained with a laser power of 12 W at an engraving speed of 200 mm/s.

a relatively narrow 2D peak, the material obtained can be identified as nanographene [30].

C. Electrical Characterization

It is well known that the conductivity of the LIG can be adjusted by controlling the level of ablation during the laser photothermal process [25], [31]. This adjustment is achieved through the laser fluence, which is determined by the different laser parameters (optical power, engraving speed, and focal distance). In this particular case, we varied the output power of the laser to 9, 10 and 12 W and ranged the engraving speed from 100 to 375 mm/s, extracting the sheet resistance for each configuration using the Jandel® 4-point probe station with the Dual-Configuration standard [32]. As shown in Fig. 4, depending on the specific configuration, the sheet resistance of the LIG can vary from 19 to 620 Ω/sq., with an average LIG thickness obtained with optical microscopy of 40 μm. Note that the laser photothermal process requires a minimum laser fluence to effectively form LIG on the surface of the polyimide. Therefore, using the higher laser power allows for both minimizing the fabrication time and maximizing the range of sheet resistance available since, as demonstrated in Fig. 4, lower laser powers are not able to form LIG at higher scanning speeds. The specific laser configuration used for

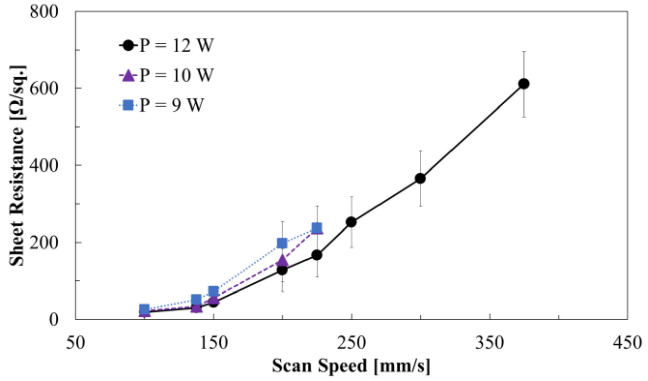

Fig. 4. Sheet resistance of the LIG. Laser power: 9, 10 and 12 W, scanning speed range: 100 to 375 mm/s.

the fabrication of the FSS structure depends on the desired sheet resistance required for the desired frequency response and therefore it is determined by the optimization process, as described in the following section.

III. Absorbing Properties Analysis

A. Electromagnetic Simulation

The simulation of the proposed structure was carried out by using the Ansys HFSS simulator. The simulation scenario considers that when an incident electromagnetic wave impinges on the lossy FSS structure, a fraction of the incident energy is directly dissipated into heat due to the inherent resistance of the surface. Additionally, the pattern alters the EM field distribution, resulting in impedance mismatches. This latter effect leads to partial reflections and scattering of the incident wave, creating absorption bands within the frequency spectrum. As a result, the FSS acts as a filter for certain frequencies [3]. The simulation was implemented by periodic boundaries and Floquet port under normal incidence, which allows to simulate the unit cell of the periodic array as the entire structure. The characterization was performed on the near-field, as it is the best approach for studying the interactions between the electromagnetic field and the material properties of the FSS structure [17], [33]. Both LIG and polyimide layers were modeled as 3D materials with their respective experimental thicknesses.

The optimization of the dimensions of the structure was performed by using the integrated optimization tools, which implement both genetic and Quasi-Newton algorithms. Specifically, the optimization process aimed to determine the appropriate thickness of the dielectric slab and the geometrical dimensions of the square patch pattern to achieve maximal absorption in the 2.4 GHz band while minimizing the overall thickness of the structure. While it was not considered in the optimization process, it would be also possible to take into account bandwidth constraints. However, it could result in limited absorption levels for a given pattern. Therefore, the use of severe constraints in all the optimization parameters may require the exploration of alternative patterns or multi-layered topologies [8], [34].

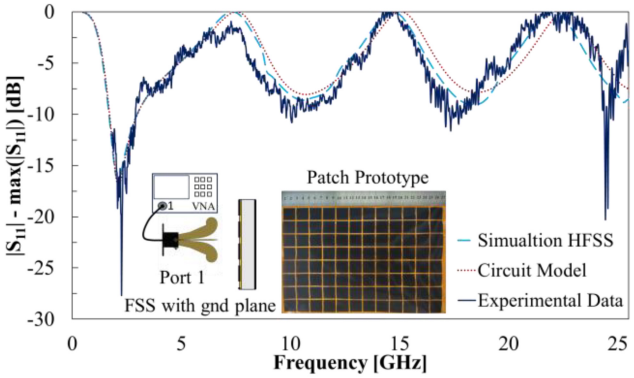

Fig. 5. Absorption (S_{11}) properties of the proposed patch LIG-FSS structure at normal incidence.

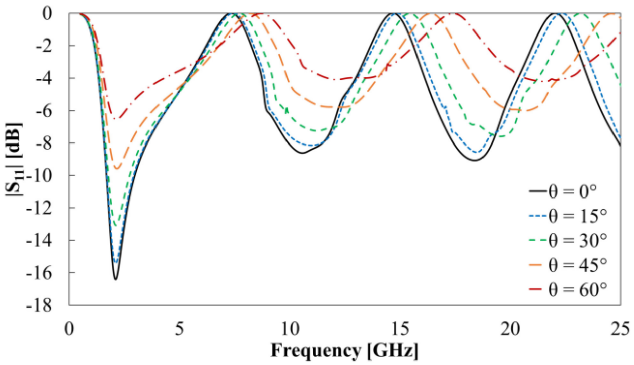

Fig. 6. Absorption simulation properties under different incident angles (θ) for TE polarization.

The optimization stage resulted in the following parameters: a thickness of the polystyrene slab of 12 mm, a cell periodicity (D) of 22.56 mm and a gap (g) of 2.05 mm with a sheet resistance of 118 Ω/sq. The HFSS simulation results included in Fig. 5 confirmed that the FSS structure presents a main absorption band at 2.4 GHz, which corresponds to the intended design, together with additional absorption bands as a result of the periodicity of the equivalent impedance of the structure.

B. Angular Stability

The angular stability of the LIG-FSS structure is also of special interest to determine how the FSS structure behaves across different incident angles, especially in the case of single-layer FSS [35]. For that, we simulated the absorption characteristic of the proposed structure under different angles (θ), as depicted in Fig. 6.

As expected, the FSS structure exhibits lower absorption and higher bandwidth as the incident angle increases as a consequence of the dependency of the constructive and destructive interferences with the incident angle. Despite this, an acceptable level of absorbance is still maintained at the frequency of interest even for $\theta = 30°$.

C. Electrical Model

According to the electromagnetic fundamental theory [8], [36], the proposed FSS absorber can be modelled as the equivalent circuit presented in **Fig. 7.**

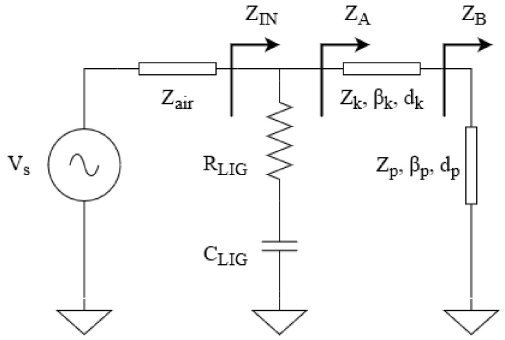

Fig. 7. Equivalent circuit of the LIG-FSS microwave absorber.

The lossy periodic pattern is modelled as a series RC circuit, where the resistive part (R_{LIG}) is derived from the pattern dimensions (1) and the lump capacitance (C_{LIG}) is associated with the gap between cells [8].

$$R_{LIG} = R_{sh}\frac{D^2}{(D-g)^2} \quad (1) \tag{1}$$

In (1) R_{sh} represents the sheet resistance of the LIG pattern, D the cell periodicity, and g the gap between patches. From (1) it can be obtained that $R_{LIG} = 155\ \Omega$ for the optimized design.

On the one hand, the grounded polystyrene dielectric slab behaves as an inductor, hence it is modelled as a short-circuit transmission line of length d_p (2). On the other hand, the polyimide film is equivalent to a transmission line of length d_k in series with Z_B (3). Finally, the lossy periodic pattern is connected in parallel with both equivalent transmission lines, and therefore, the equivalent input impedance of the structure can be expressed as (4).

$$Z_B = jZ_p\tan(\beta_p d_p) \tag{2}$$

$$Z_A = Z_k\frac{Z_B + jZ_k\tan(\beta_k d_k)}{Z_k - jZ_B\tan(\beta_k d_k)} \tag{3}$$

$$Z_{IN} = \left(R_{LIG} - \frac{j}{\omega C_{LIG}}\right)\|\ Z_A \tag{4}$$

In these equations, ω is the angular frequency. Z_p and Z_k are the intrinsic impedances of the polystyrene and the polyimide layers respectively, while β_p and β_k are their wavenumbers (also known as repetency). These parameters depend on the relative permittivity (ε_r) and permeability (μ_r) of each material as presented in (5) and (6).

$$Z_i = \sqrt{\frac{\mu_{r_i}\mu_0}{\varepsilon_{r_i}\varepsilon_0}} \quad i = p, k \tag{5}$$

$$\beta_i = \omega\sqrt{\varepsilon_{r_i}\varepsilon_0\mu_{r_i}\mu_0} \quad i = p, k \tag{6}$$

In this particular case, the relative permittivity is $\varepsilon_{r,p} = 2.6$ and $\varepsilon_{r,k} = 3.5$, while the relative permeabilities are $\mu_r = 1$ for both materials.

According to the transmission line theory, the reflection parameter S_{11} can be obtained by the relation between the input impedance and the characteristic impedance of air, as described in (7).

$$S_{11} = \frac{Z_{IN} - Z_{air}}{Z_{IN} + Z_{air}} \tag{7}$$

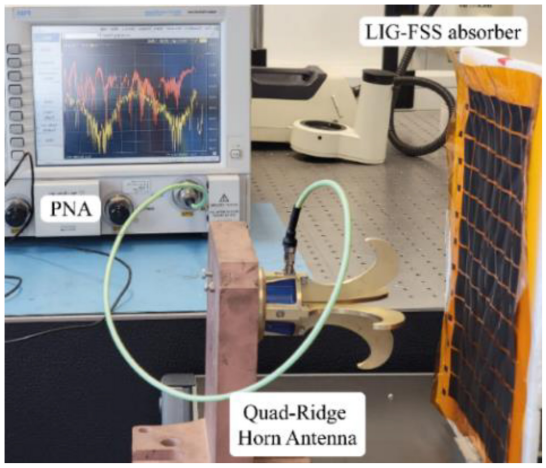

Fig. 8. Measurement setup for the absorption properties of the LIG-FSS.

Therefore, the absorption coefficient can be estimated as:

$$A = 1 - |S_{11}|^2 - |S_{21}|^2 \tag{8}$$

where S_{21} refers to the transmission parameter [37]. As seen, the absorption coefficient depends on the frequency, but also on the thickness (d_p, d_k), permittivity, and permeability (ε_r, μ_r) of both substrates and the lossy pattern dimensions.

Using these parameters, C_{LIG} was obtained by fitting the model to the HFFS simulation results, which resulted in an equivalent capacitance of $C_{LIG} = 0.52$ pF. The simulation results of the final electrical model are also included in Fig. 5, which are in good agreement with the simulation results. This model describes the basic principle of the proposed single-layer FSS structure. In the classical Salisbury screen, the resonance occurs when the inductive impedance of the grounded dielectric slab and the capacitive impedance of the resistive non-patterned surface have the same magnitude; then the imaginary part cancels each other, and the real part contributes to the losses. In that case, it would only happen at the frequency defined by the thickness of the dielectric ($\lambda/4$). However, in this case, this limitation is surpassed thanks to the additional capacitance added by the gaps between adjacent resistive square patches [8].

IV. Experimental Results

A LIG-FSS microwave absorber prototype was fabricated according to the optimized dimensions. The size of the structure was 264 × 175 mm, consisting of 12 × 8 square patch arrays, with a total thickness of 12 mm. The reflection coefficient of the LIG-FSS structure was measured in the near-field with a Quad-Ridge horn QH2000 antenna connected to the PNA N5222A Microwave Network Analyzer from Keysight Technologies®, as depicted in Fig. 8.

A. Optimized Patch Design

The experimental results obtained for the patch LIG-FSS absorber are displayed in Fig. 5 together with the results of the EM simulation and the equivalent electrical circuit. Note that the experimental results are limited to 2 GHz since it is the minimum operating frequency of the antenna used. The different results show a good agreement for the four absorption bands, which are located around 2.3, 10.1, 17.7, and 24.6 GHz. The first absorption peak, for which the design has been optimized, exhibits an absorption magnitude that exceeds 90% over a bandwidth of 1.22 GHz (from 1.69 to 2.91 GHz) obtaining a relative bandwidth of 53% computed as:

$$\text{RB} = 2\frac{f_H - f_L}{f_H + f_L} \tag{9}$$

being f_H and f_L the upper and the lower frequency for 90% of absorption. Note also that the total thickness (12 mm) corresponds only to a $0.068\cdot\lambda$ at the lowest operating frequency of the absorber. The slight differences between experimental and simulation results can be explained by the small deformations on the polyimide film caused by the heat induced during the fabrication, the variability of the sheet resistance, and other experimental mismatches.

TABLE I
Comparison of Microwave Absorbers Based on Single-Layer FSS

Relative Bandwidth	Absorption	Thickness	Ref
97% (4.5-13 GHz)	90%/10 dB	$0.11\cdot\lambda_{max}$	[8]
97% (7.1-20.6 GHz)	90%/10 dB	$0.12\cdot\lambda_{max}$	[39]
60% (8.5-16 GHz)	90%/10 dB	$0.067\cdot\lambda_{max}$	[40]
39% (1.22-1.81 GHz)	99%/20 dB	$0.2\cdot\lambda_{max}$	[41]
53% (1.69-2.91 GHz)	90%/10 dB	$0.068\cdot\lambda_{max}$	Our work

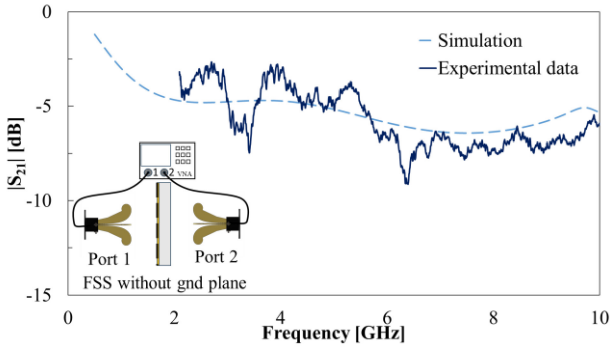

Fig. 9. Transmission properties of the proposed patch LIG-FSS structure without ground plane.

Table I compares our proposed absorber with other absorbers based on a single-layer FSS. As observed, the FSS absorber proposed in this study exhibits a narrower bandwidth and minimal thickness for the frequency of interest, being 62% thinner than the traditional Salisbury screen with equivalent absorption outcomes [38]. It is noteworthy that this narrower bandwidth is achieved with the simple patch pattern, in contrast to other absorbers employing more complex shapes and larger dielectric materials to obtain broader bandwidths. Additionally, our absorber offers the added advantage of a maskless, chemical-free, single-step fabrication process with adjustable sheet resistance, which can be used to tune the absorber bandwidth (as demonstrated in Section IV-B).

In addition to the S_{11} absorption coefficient, Fig. 9 presents the EM simulation and the measurement of the S_{21} transmission coefficient of the LIG-FSS patch absorber. In this

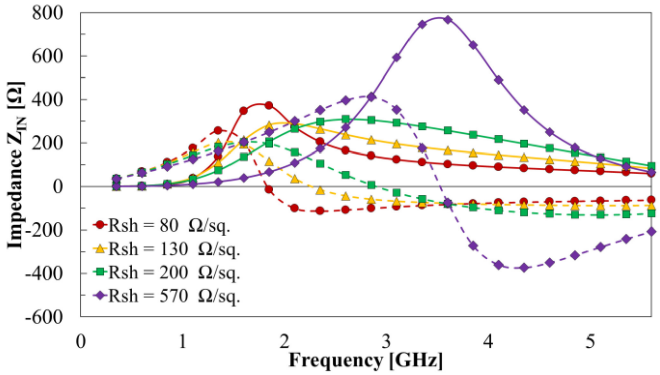

Fig. 10. Real and imaginary parts of the input impedance for different sheet resistances.

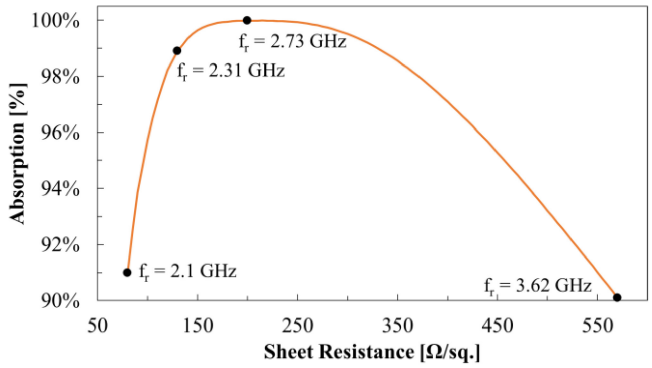

Fig. 11. Absorption of the proposed patch absorber for different sheet resistances. The resonant frequencies for 80, 130, 200, 570 Ω/sq. are also indicated.

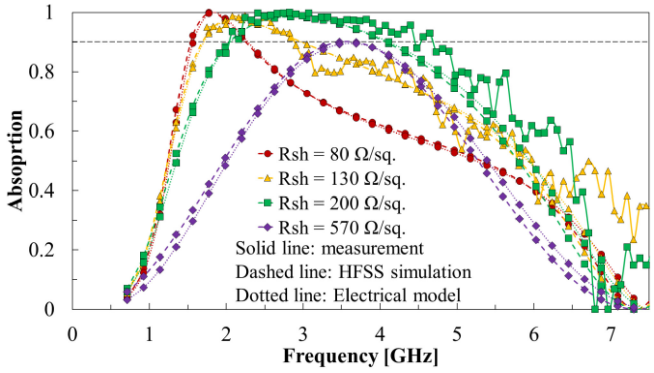

Fig. 12. Absorption coefficient of the proposed microwave absorber for different sheet resistances.

configuration (depicted in the inset of Fig. 9), the ground plane is removed, and the structure is placed between two Quad-Ridge Horn Antennas [42], resulting in a transmission level of around −5 dB. Again, a good agreement is found with simulation results, which confirms the validity of our approach.

B. Tunable Characteristics

As demonstrated in Section II, the resistivity of the LIG pattern can be easily tuned by adjusting the laser parameters. Therefore, according to (4), it can be used to tune the input impedance (Z_{IN}), thereby influencing the resonant frequency (f_r) of the absorber, defined as the frequency that cancels the imaginary part of the input impedance (10). This feature is demonstrated in Fig. 10, where the dependency of the real and imaginary parts of input impedance is plotted as a function of the frequency for different sheet resistances (80, 130, 200, and 570 Ω/sq.).

$$\mathrm{Im}\{Z_{IN}(f_r, R_{sh})\} = 0 \tag{10}$$

At the resonance frequency, the incident microwave energy is primarily absorbed rather than reflected by the absorber, hence a significant portion of the incoming electromagnetic wave energy is converted into heat due to the inherent resistance of the surface [4]. As a result, the S_{11} response presents the absorption peak observed at f_r (Fig. 5). Therefore, the position of the absorptive peak can be easily tuned by modifying the sheet resistance of the LIG. This is demonstrated in Fig. 11, where we can observe that the resonance frequency of the proposed FSS structure can be tuned from 2.1 GHz to 3.62 GHz (span of 1.52 GHz), while maintaining a high absorption characteristic of over 90% of absorption without modifying the design dimensions. For that, the real part of the input impedance is required to be in the range defined in (11), which can be achieved for a wide range of sheet resistances (from 80 to 570 Ω/sq.), thus demonstrating that the FSS absorber is quite robust to possible variabilities in the fabrication process.

$$0.52 \cdot Z_{air} < \mathrm{Re}\{Z_{in}(f_r, R_{sh})\} < 1.92 \cdot Z_{air} \tag{11}$$

However, tuning the frequency response using the same design dimensions also affects the selectivity of the absorber. This effect is presented in Fig. 12 for different sheet resistances (80, 130, 200, and 570 Ω/sq.) along with the experimental results for 130 and 200 Ω/sq. As seen, the increase in the sheet resistance leads to the shifting of the frequency of resonance, but also to a wider bandwidth. In particular, the experimental results for 130 and 200 Ω/sq. reveal a shift of the resonant frequency from 2.3 to 2.7 GHz with a 2.13 factor increase in bandwidth.

These results, together with the good agreement between simulation, equivalent circuit, and experimental results demonstrate the feasibility of tuning the frequency response of the absorber in a much simpler way when compared to other fabrication approaches, such as metal-based FSS.

C. Square Ring Pattern

Finally, this section exemplifies the versatility of the laser photothermal process for the fabrication of LIG-FSS with more advanced patterns without the necessity to include any additional fabrication step. In this way, many different frequency responses can be achieved by modifying the laser-scribed pattern on the surface of the polyimide [43]. For instance, here we include the results obtained for a resistive square ring pattern (Fig. 13). This type of shape enables the creation of a multi-resonant FSS, potentially leading to increased bandwidth and improved angular stability. In this scenario, the inclusion of the ring-shaped pattern introduces an additional equivalent inductive impedance (L_{LIG}). Consequently, a secondary parallel resonance emerges between the FSS and the grounded substrate when the

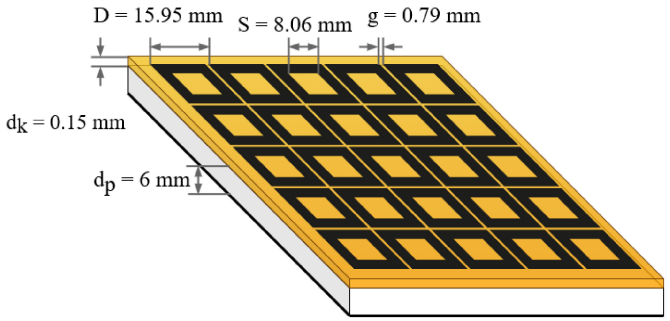

Fig. 13. Structure of the proposed square ring LIG-FSS.

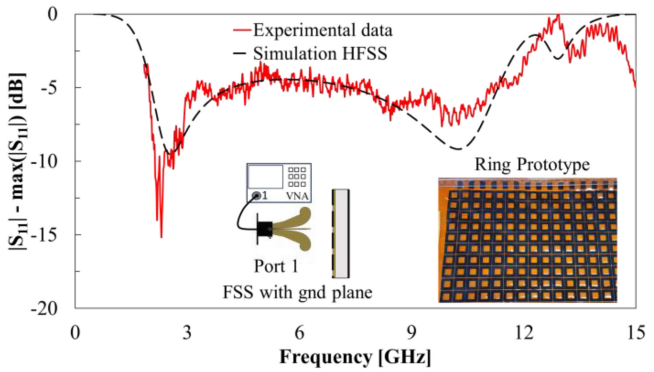

Fig. 14. Absorption ($|S_{11}|$) properties of the proposed square ring LIG-FSS structure at normal incidence.

inductive impedance of the FSS aligns with the capacitive impedance of the dielectric slab [7].

In this case, the optimized LIG-FSS dimensions are the following: a thickness of the polystyrene slab of 6 mm, a cell periodicity (D) of 15.95 mm, a gap (g) of 0.79 mm and a side for the inner square (S) of 8.06 mm, with a sheet resistance of 33.8 Ω/sq. Consequently, the prototype was built using a laser power of 12 W at an engraving speed of 140 mm/s. Using the characterization setup presented in Fig. 8, the new square ring LIG-FSS was validated with respect to the HFSS simulation results, revealing a good match in the frequency response with a main absorption peak at 2.5 GHz and an additional absorption band at 10.2 GHz, as shown in Fig. 14.

V. Conclusion

This study introduces a pioneer absorptive Frequency Selective Surface (FSS) using Laser-Induced Graphene (LIG) as the resistive material. It is demonstrated that this technique enables the creation of tunable, thin, lightweight, sustainable, and cost-effective microwave absorbers. Electromagnetic simulations and circuital modeling were carried out to optimize and evaluate the absorption properties of the proposed absorber. In addition, various LIG-FSS prototypes were fabricated and tested in the near-field under real conditions, demonstrating a good agreement with the simulation results. The controllable resistivity of LIG, achieved through precise adjustments of laser parameters, proves the tunability of the LIG-FSS absorber. These findings confirm the potential of LIG-FSS for the fabrication of thin lightweight and sustainable microwave absorbers with adjustable properties.

References

[1] E. F. Knott, J. F. Schaeffer, and M. T. Tulley, *Radar Cross Section*. Raleigh, NC, USA: SciTech Publ., 2004.

[2] J. Jia, H. Liang, G. Chen, and L. Zhang, "A review on one-dimensional carbon-based composites as electromagnetic wave absorbers," *J. Mater. Sci., Mater. Electron.*, vol. 33, pp. 567–584, Jan. 2022.

[3] B. A. Munk, *Frequency Selective Surfaces: Theory and Design*. Hoboken, NJ, USA: Wiley, 2005.

[4] D. Yi, X.-C. Wei, and Y.-L. Xu, "Tunable microwave absorber based on patterned graphene," *IEEE Trans. Microw. Theory Techn.*, vol. 65, no. 8, pp. 2819–2826, Aug. 2017.

[5] F. Bayatpur and K. Sarabandi, "A tunable metamaterial frequency-selective surface with variable modes of operation," *IEEE Trans. Microw. Theory Techn.*, vol. 57, no. 6, pp. 1433–1438, Jun. 2009.

[6] J. Yang, J. Chen, L. Quan, Z. Zhao, H. Shi, and Y. Liu, "Metamaterial-inspired optically transparent active dual-band frequency selective surface with independent wideband tunability," *Opt. Exp.*, vol. 29, no. 17, pp. 27542–27553, 2021.

[7] M. Li, B. Muneer, Z. Yi, and Q. Zhu, "A broadband compatible multi-spectral metamaterial absorber for visible, near-infrared, and microwave bands," *Adv. Opt. Mater.*, vol. 6, no. 9, 2018, Art. no. 1701238.

[8] F. Costa, A. Monorchio, and G. Manara, "Analysis and design of ultra thin electromagnetic absorbers comprising resistively loaded high impedance surfaces," *IEEE Trans. Antennas Propag.*, vol. 58, no. 5, pp. 1551–1558, May 2010.

[9] M. Haghzadeh and A. Akyurtlu, "All-printed, flexible, reconfigurable frequency selective surfaces," *J. Appl. Phys.*, vol. 120, no. 18, 2016, Art. no. 184901.

[10] R. S. Anwar, L. Mao, and H. Ning, "Frequency selective surfaces: A review," *Appl. Sci.*, vol. 8, no. 9, p. 1689, 2018.

[11] R. Mishra, A. Sahu, and R. Panwar, "Cascaded graphene frequency selective surface integrated tunable broadband terahertz metamaterial absorber," *IEEE Photonics J.*, vol. 11, no. 2, pp. 1–10, Apr. 2019.

[12] A. A. Dewani, S. G. O'Keefe, D. V. Thiel, and A. Galehdar, "Optically transparent frequency selective surfaces on flexible thin plastic substrates," *AIP Adv.*, vol. 5, no. 2, 2015, Art. no. 027107.

[13] J. Lorenzo, A. Lázaro, R. Villarino, and D. Girbau, "Modulated frequency selective surfaces for wearable RFID and sensor applications," *IEEE Trans. Antennas Propag.*, vol. 64, no. 10, pp. 4447–4456, Oct. 2016.

[14] A. M. J. Marindra and G. Y. Tian, "Chipless RFID sensor for corrosion characterization based on frequency selective surface and feature fusion," *Smart Mater. Struct.*, vol. 29, no. 12, 2020, Art. no. 125010.

[15] S. Milici, J. Lorenzo, A. Lazaro, R. Villarino, and D. Girbau, "Wireless breathing sensor based on wearable modulated frequency selective surface," *IEEE Sensors J.*, vol. 17, no. 5, pp. 1285–1292, Mar. 2017.

[16] D. Le, L. Ukkonen, and T. Björninen, "A dual-ID RFID tag for headgear based on quasi-Yagi and dipole antennas," *IEEE Antennas Wireless Propag. Lett.*, vol. 19, pp. 1321–1325, 2020.

[17] S. Sharma, M. R. Tripathy, and A. K. Sharma, "High gain FSS integrated slotted UHF RFID antenna for WBAN," *Int. J. Syst. Assurance Eng. Manag.*, vol. 14, pp. 610–621, Sep. 2021.

[18] A. Lazaro, A. Ramos, D. Girbau, and R. Villarino, "A novel UWB RFID tag using active frequency selective surface," *IEEE Trans. Antennas Propag.*, vol. 61, no. 3, pp. 1155–1165, Mar. 2013.

[19] A. Jiménez-Sáez et al., "Frequency selective surface coded retroreflectors for chipless indoor localization tag landmarks," *IEEE Antennas Wireless Propag. Lett.*, vol. 19, pp. 726–730, 2020.

[20] S. Sharma, M. R. Tripathy, and A. K. Sharma, "High gain passive UHF RFID reader antenna using novel FSS for longer read range," *IETE J. Res.*, 2023, to be published.

[21] K. ElMahgoub and T. Navigation, "Frequency selective surfaces for UHF RFID applications," in *Proc. IEEE Int. Symp. Antennas Propag. USNC/URSI Nat. Radio Sci. Meet.*, 2015, pp. 987–988.

[22] J. Lin et al., "Laser-induced porous graphene films from commercial polymers," *Nat. Commun.*, vol. 5, no. 1, p. 5714, 2014.

[23] F. J. Romero et al., "Inexpensive and flexible nanographene-based electrodes for ubiquitous electrocardiogram monitoring," *NPJ Flexible Electron.*, vol. 3, no. 1, p. 12, 2019.

[24] B. Sindhu, A. Kothuru, P. Sahatiya, S. Goel, and S. Nandi, "Laser-induced graphene printed wearable flexible antenna-based strain sensor for wireless human motion monitoring," *IEEE Trans. Electron Devices*, vol. 68, no. 7, pp. 3189–3194, Jul. 2021.

[25] Y. Houeix et al., "Laser-synthesis of conductive carbon-based materials from two flexible commercial substrates: A comparison," *Appl. Surface Sci.*, vol. 634, Oct. 2023, Art. no. 157629, doi: 10.1016/j.apsusc.2023.157629.
[26] A. Salvia, A. Mostaccio, G. Antonelli, E. Martinelli, and G. Marrocco, "Full-LIG wireless batteryless sensor for the detection of amines," in *Proc. IEEE Int. Conf. Flexible Printable Sensors Syst. (FLEPS)*, 2023, pp. 1–4.
[27] A. Mostaccio, A. Salvia, G. Antonelli, E. Martinelli, and G. Marrocco, "Laser-induced graphene fan antenna for RFID applications," in *Proc. IEEE 13th Int. Conf. RFID Technol. Appl. (RFID-TA)*, 2023, pp. 25–28.
[28] Y. Houeix, F. J. Romero, D. P. Morales, N. Rodriguez, and D. Kaddour, "Novel frequency selective surface made of laser-induced graphene," in *Proc. IEEE 13th Int. Conf. RFID Technol. Appl. (RFID-TA)*, 2023, pp. 257–260, doi: 10.1109/RFID-TA58140.2023.10290670.
[29] R. Mukherjee, A. V. Thomas, A. Krishnamurthy, and N. Koratkar, "Photothermally reduced graphene as high-power anodes for lithium-ion batteries," *ACS Nano*, vol. 6, no. 9, pp. 7867–7878, 2012.
[30] I. Childres, L. A. Jauregui, W. Park, H. Cao, and Y. P. Chen, "Raman spectroscopy of graphene and related materials," *New Develop. Photon Mater. Res.*, vol. 1, pp. 1–20, Jan. 2013.
[31] F. J. Romero et al., "In-depth study of laser diode ablation of Kapton polyimide for flexible conductive substrates," *Nanomaterials*, vol. 8, no. 7, p. 517, 2018.
[32] "Standard test method for sheet resistance uniformity evaluation by in-line four-point probe with the dual-configuration procedure," *Amer. Soc. Test. Mater.*, vol. 10.04, p. 13, Dec. 1997, doi: 10.1520/F1529-02.
[33] X. L. Chang, P. S. Chee, and E. H. Lim, "Compact conformal tattoo-polymer antenna for on-body wireless power transfer," *Sci. Rep.*, vol. 13, no. 1, pp. 1–12, 2023.
[34] Z. Yao, S. Xiao, Y. Li, and B.-Z. Wang, "On the design of wideband absorber based on multilayer and multiresonant FSS array," *IEEE Antennas Wireless Propag. Lett.*, vol. 20, pp. 284–288, 2020.
[35] T. Hong, W. Xing, Q. Zhao, Y. Gu, and S. Gong, "Single-layer frequency selective surface with angular stability property," *IEEE Antennas Wireless Propag. Lett.*, vol. 17, pp. 547–550, 2018.
[36] F. Costa, A. Monorchio, and G. Manara, "Efficient analysis of frequency-selective surfaces by a simple equivalent-circuit model," *IEEE Antennas Propag. Mag.*, vol. 54, no. 4, pp. 35–48, Aug. 2012.
[37] D. Kundu, A. Mohan, and A. Chakrabarty, "Single-layer wideband microwave absorber using array of crossed dipoles," *IEEE Antennas Wireless Propag. Lett.*, vol. 15, pp. 1589–1592, 2016.
[38] B. Chambers, "Optimum design of a salisbury screen radar absorber," *Electron. Lett.*, vol. 30, no. 16, pp. 1353–1354, 1994.
[39] W. Li, H. Jin, Z. Zeng, L. Zhang, H. Zhang, and Z. Zhang, "Flexible and easy-to-tune broadband electromagnetic wave absorber based on carbon resistive film sandwiched by silicon rubber/multi-walled carbon nanotube composites," *Carbon*, vol. 121, pp. 544–551, Sep. 2017.
[40] A. Sharma, R. Panwar, and R. Khanna, "Experimental validation of a frequency-selective surface-loaded hybrid metamaterial absorber with wide bandwidth," *IEEE Magn. Lett.*, vol. 10, pp. 1–5, 2019.
[41] D. Ye et al., "Ultrawideband dispersion control of a metamaterial surface for perfectly-matched-layer-like absorption," *Phys. Rev. Lett.*, vol. 111, no. 18, 2013, Art. no. 187402.
[42] R. Jaiswar, F. Mederos-Henry, V. Dupont, S. Hermans, J.-P. Raskin, and I. Huynen, "Inkjet-printed frequency-selective surfaces based on carbon nanotubes for ultra-wideband thin microwave absorbers," *J. Mater. Sci., Mater. Electron.*, vol. 31, no. 3, pp. 2190–2201, 2020.
[43] A. Kapoor, R. Mishra, and P. Kumar, "Frequency selective surfaces as spatial filters: Fundamentals, analysis and applications," *Alexandria Eng. J.*, vol. 61, no. 6, pp. 4263–4293, 2022.

Yann Houeix (Student Member, IEEE) received the B.Eng. and M.Eng. degrees in electronic engineering from the University of Granada, Spain, in 2020 and 2021, respectively, where he is currently pursuing the Ph.D. degree funded by a National Fellowship with the Pervasive Electronics Advanced Research Laboratory. Additionally, in 2019, he was an exchange student at master level with the École Polytechnique Federal de Lausanne. His current research interests include flexible electronics for sensor application and RFID technology with novel materials.

Francisco J. Romero received the B.Eng. degree (with Hons.) and the M.Eng. degree (with Hons.) in telecommunications engineering from the University of Granada, Spain, in 2016 and 2018, respectively, and the Ph.D. degree, funded by a national fellowship, in flexible and printed electronics from the University of Granada in collaboration with the Technical University of Munich, Germany, in 2021. In 2015, he joined the Department of Electronics and Computer Technology, University of Granada as an Ungraduated Researcher. Following his Ph.D. degree, he served as an R&D Team Leader with Eesy-Innovation, and he is currently a Postdoctoral Researcher with the University of Granada. His research interests include flexible and printed electronics, graphene-based materials, and IoT embedded systems.

Francisco G. Ruiz received the Telecommunication Engineering degree from the University of Malaga in 2002, and the Ph.D. degree in physics from the University of Granada, Spain, in 2005. Since 2006, he has been with the Department of Electronics, University of Granada, where he co-founded the Pervasive Electronics Advanced Research Laboratory in 2018. He was a Visiting Researcher with TUDelft, UCL, IMEC, and Universität Siegen. His research focuses on 2-D materials-based electron devices, including RF devices and circuits, sensors, optoelectronic devices, and neuromorphic devices and circuits.

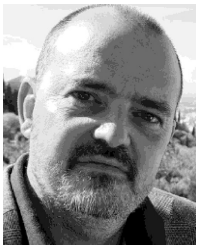

Diego P. Morales received the B.Sc. and M.Eng. degrees in electronics engineering in 2001 and the Ph.D. degree from the University of Granada. In 2001, he was working with Infineon Technologies AG, Munich, Germany, when he obtained a position as a Professor with the University of Almería, Spain. In 2006, he joined the University of Granada, where he is currently a Full Professor of Electronics with the Department of Electronics and Computer Technology. He has headed several national and international projects, 20 company contracts, coauthored one international patents, more than 90 peer-reviewed scientific journal's articles, and multiple international congress contributions. In addition, he has supervised eight Ph.D. Theses (seven of them industrial thesis in several European companies: Infineon Technologies AG, HAT.tec GmbH, eesy-Innovation GmbH) and cofounded RedNodeLabs UG in 2020. His current research interests include power electronics (circuits control and systems), low-power energy conversion and transmission, and new materials and devices for electronic applications.

Noel Rodriguez received the B.Sc. and M.Eng. degrees in electronics engineering from the University of Granada, with First National Award of University Education in 2004, and a dual awarded Ph.D. degree from the University of Granada and the National Polytechnic Institute of Grenoble, France, in 2008. From 2017 to 2020, he was the Head of the Pervasive Electronics Advanced Research Laboratory, University of Granada, where he is currently a Full Professor of Electronics with the Department of Electronics and Computer Technology. He has headed over 15 national and international projects, eight company contracts, coauthored 15 international patents, several book chapters, and more than 150 peer-reviewed scientific contributions. His current research interests include power electronics, low-power energy conversion and transmission, and new materials and devices for electronic applications.

Darine Kaddour (Member, IEEE) was born in Mechmech, Lebanon, in February 1982. She received the B.S. degree in physics from the Faculty of Sciences, Lebanese University, Tripoli, Lebanon, in 2003, and the M.S. and Ph.D. degrees from the Institut National Polytechnique de Grenoble, Grenoble, France, in 2004 and 2007, respectively. Since, 2009, she has been an Assistant Professor with the LCIS Laboratory, Valence, France, where her research interests include microwave circuits and radio-frequency identification antennas.